

When holography meets coherent diffraction imaging

Tatiana Latychevskaia*, Jean-Nicolas Longchamp and Hans-Werner Fink

Physics Institute

University of Zurich

Winterthurerstrasse 190

8057 Zurich

Switzerland

Corresponding author:

e-mail: tatiana@physik.uzh.ch

Abstract

Phase problem exists in crystallographic, astronomical and optical imaging where only the intensity of the scattered signal is detected and the phase information is lost and must somehow be recovered to reconstruct the object's structure. The modern imaging techniques rely on implementation of novel coherent light sources like X-ray free electron lasers with the ultimate goal of visualize such objects as individual biomolecules rather than crystals. Here, unlike in case of crystals where structure can be solved by model building and phase refinement, the phase distribution of the wave scattered by an individual molecule must be recovered directly. There are two well-known solutions to the phase problem: holography and coherent diffraction imaging (CDI). Both techniques have their pros and cons. In holography, the reconstruction of the scattered complex-valued object wave is directly provided by a well-defined reference wave that must cover the entire detector area which often is an experimental challenge. CDI provides highest

possible, only wavelength limited, resolution, but the phase recovery is an iterative process which requires some pre-defined information about the object and whose outcome is not always uniquely-defined. Moreover, the diffraction patterns must be recorded under oversampling conditions even to be able to solve the phase problem. We report here how holography and CDI can be merged into one superior technique: holographic coherent diffraction imaging (HCDI). An inline hologram can be recorded by employing a modified CDI experimental scheme. It is demonstrated that the amplitude of the Fourier transform of the inline hologram is relevant to the complex-valued visibility, thus providing information on both, amplitude and the phase in the diffraction pattern plane. With the phase information available, the condition of oversampling of diffraction patterns becomes obsolete, and the phase problem can be solved fast and unambiguous. We demonstrate reconstruction of objects recorded with optical wave and low-energy electrons with our new method. The proposed here method can be realized with any other type of radiation, such as high-energy electrons or X-rays.

PACS: 42.30.Rx, 42.40.-i, 61.05.cp, 61.05.jp

I. INTRODUCTION

The so-called phase problem exists in crystallographic, astronomical and optical imaging, or more general, in all scattering experiments independent of the radiation used. The distribution of the scattered wave is complex-valued with the phase part carrying information about individual scattering events, hence about the positions of elements constituting the object. The trouble is that the detector records only the intensity, i.e. the square of the amplitude of the scattered wave and, since no phase sensitive detector

exists, the phase information is lost but must somehow be recovered to reconstruct the object's arrangement. A remarkable example of the phase problem is the famous discovery of the DNA double helix based on its X-ray diffraction pattern. It needed the chemical intuition of Watson, Crick and others accompanied by extensive model building to eventually end up with the structure of the DNA double helix. Such guessing would not be necessary if the diffraction pattern had not only amplitude but also phase information.

Modern trends in structural biology, as exemplified also by the recent developments of powerful X-ray lasers, aim at imaging just one individual molecule. In this way one shall avoid averaging over a large number of molecules whereby structural information related to conformational flexibility of the proteins is lost. In the case of just one individual molecule, periodicity and with this symmetry relations as in crystals are gone and therefore, for imaging a single molecule, a true solution to the phase problem is as important as ever.

Up to date there are two well-studied solutions to the phase problem, in order of historical appearance: holography [1] and coherent diffraction imaging (CDI) [2]. Holography was invented by Dennis Gabor in 1947 [1, 3] when he tried to improve the resolution in electron microscope. In Gabor's scheme, an object is placed into divergent wave (reference wave) and part of the wave is scattered by the object (object wave), both waves interfere at the detector thus forming a hologram. Since both reference and object wave share the same optical axis, this type of holography is called inline. The reconstruction of the scattered complex-valued object wave is straight forward and provided by a well-defined reference wave that must cover the entire detector area which

often is an experimental challenge. In CDI a plane wave incidents an object and the scattered wave is detected in the far-field. No lenses are used between the sample and the detector, and as the result: (a) not the image of the object but its diffraction pattern is formed in the detector plane, and (b) highest possible resolution [4] can be achieved. CDI, however, requires a retrieval of the phase distribution, which is conventionally achieved by an iterative reconstruction procedure provided some information about the object is available [5]. The envisioned ultimate application of the CDI is obtaining an image of an individual biological molecule at atomic resolution. Biological specimens have already been imaged by CDI employing coherent X-rays: *E.coli* bacteria was imaged with 2 Å X-rays at a resolution of 30 nm by J. Miao et al. [6]; unstained yeast cell was imaged with 1.7 nm X-rays at a resolution of 30 nm by D. Shapiro et al. [7] and single herpesvirus virions were imaged with 2.5Å X-rays at a resolution of 22 nm by C. Song et al. [8]; the first results from the Linac Coherent Light Source X-FEL facility reported imaging an individual unstained mimivirus with 6.9 Å X-rays and reconstructed at 32 nm resolution [9].

Here, we show how holography and CDI can be merged into one superior technique: holographic coherent diffraction imaging (HCDI), which inherits the benefits of both techniques, such as straightforward unambiguous recovery of the phase distribution and visualization of a non-crystalline object at highest possible resolution.

II. PHASE RECOVERY BY CDI

In CDI, a plane wave is scattered by an object and the intensity distribution at a plane right behind an object is described as the exit wave $t(x,y)$. The distribution of the

scattered wave in the far-field is given by the Fourier-transform of the exit wave and represents complex-valued visibility $V(X,Y) = \text{FT}[t(x,y)]$. Here, (x,y) and (X,Y) are the coordinates in the object and detector plane respectively. The measured intensity, or diffraction pattern, is given by $I(X,Y) = |V(X,Y)|^2$. In 1952 Sayre [10], who was investigating crystallographic imaging at the time, published half-a-page article named “Some implications of a theorem due to Shannon”. Sayre addressed published shortly before sampling theorem by Shannon [11] and noted that the structure, whose Fourier spectrum corresponds to $| \text{FT}[t(x,y)] |^2$ is the Patterson map of a single unit, this structure also has the size twice the width of the unit cell. Therefore, if $| \text{FT}[t(x,y)] |^2$ is sampled at double the Nyquist frequency (later called as “oversampling”), the recovery of structure of a crystal unit cell from X-ray diffraction pattern alone is in principle possible. But in Sayre’s own words “the paper did not, however, suggest an effective way of obtaining such sampling” [12], and neither it suggested an algorithm for reconstruction of such images. The first algorithm of phase recovery from diffraction pattern came from electron microscope imaging. In 1972 Gerchberg and Saxton [13] proposed a practical algorithm of recovery of the complex-valued wavefront from two intensity measurements (that are feasible to obtain in a TEM): in the object and diffraction planes. Here, the diffraction pattern did not have to be oversampled. Gerchberg and Saxton proposed an iterative procedure of phase recovery by propagating the complex-valued wavefront between object and diffraction planes and replacing the iterated amplitudes by the measured amplitudes at each iteration. Though it was the first practical algorithm for phase recovery, the Gerchberg and Saxton (GS) algorithm in its original form has been often criticized as “not entirely satisfactory, since neither its convergence nor its

uniqueness is guaranteed a priori” [14] and so, many different enhanced variations of the GS algorithm were proposed. One of the most impactful improvement of the GS algorithm was proposed in 1978 by Fienup [15], who addressed more common experimental situation when only diffraction pattern is available and some information about the object is available, such as: the object is real, positive and localized (true for most applications, for instance, in astronomy). Fienup proposed two iterative algorithms: error-reduction (ER) algorithm, whose name reflects the fact that the error is decreasing during the iteration process. The other algorithm, named input-output (IO) algorithm, included a feedback parameter in the iterative loop, and demonstrated drastically faster convergence than the original GS algorithm. Most of the modern phase retrieval algorithms are based on the Fienup’s iterative routines, but there is still an intense search for faster algorithms that provide unambiguously defined solution [16-17].

A. Uniqueness of the solution

One of the important issues in CDI is the uniqueness of the found solution. Since according to Wiener-Khinchin theorem, the power spectrum of a signal is the Fourier transform of its autocorrelation [18-19], some authors address phase retrieval problem as the problem of finding signal distribution from its autocorrelation function. It was demonstrated in 1964 by Hofstetter [20] that for one-dimensional case there is an infinite number of functions, all of which have the same autocorrelation. Thus, there is no unique solution to one-dimensional phase retrieval problem. In 1976 Huiser et al. in 1976 [21-22] studied uniqueness of solution to two-dimensional phase problem found by GS algorithm. The conclusion was that, except for the case of two-fold ambiguity for symmetrical objects, the unique solution can be retrieved. After Fienup’s algorithms were

reported in 1978 [15], the issue of finding a unique solution of two-dimensional real and positive distribution from its auto-correlation function had been studied by Bruck and Sodin [23], and Bates et al. [24-25]. It was found that the unique solution can be found provided the diffraction pattern is “oversampled by a factor of 2 if there is to be any hope of recovering phase” as (Bates et al. [24]), or more general, the diffraction pattern must be oversampled at least twice as fine as Nyquist frequency in each dimension [25-26]. However, the presence of noise in experimental images often leads to non-unique solutions or to the stagnation of the iterative reconstruction process at some partly reconstructed object [27]. In practice, results of hundreds of iterative runs are required, which are subsequently averaged or the best ones are subjectively defined as the correct reconstructions [28-30].

B. Complex-valued objects

Initially and for a long time, the phase problem was addressing crystallographic and astronomical applications, and the constraints of objects being real and positive (electron density distribution probed by X-rays or brightness of stars) seemed logical. However, later on CDI was applied for imaging specimens whose interaction with the radiation could only be described by a complex-valued transmission function (as for instance, when a cell is imaged by soft X-rays [7]). Thus, the phase retrieval problem had to consider complex-valued objects not just as a mathematical exercise but as a practical problem. In 1984 Barakat and Newsam [31] mathematically studied the phase problem for complex-valued variables and showed that multiplicity of the found solution is pathologically rare. In 1985 Bates and Tan [32] showed that positivity constraint is (unfortunately) much more effective than support constraint, and that the phase objects

recovered by only using a support constraint are “barely recognizable” when compared to original distribution. In 1987 Fienup [33] demonstrated that some special-shaped complex-valued objects can be reconstructed using object-contour-tight support. Meanwhile, it has become a common knowledge that complex-valued objects can be reconstructed when the support is accurately known, and the support boundaries are as sharp as possible [34].

C. Other issues in CDI

There are several other problems associated with the CDI method. The phase retrieval is only possible when diffraction pattern is oversampled. Thus, the geometry of the experimental setup must be designed to fulfill the oversampling condition. As a consequence, one would rather record an “oversampled” diffraction pattern than diffraction pattern showing higher order diffraction. Next, the oversampling condition in detector plane corresponds to zero-padding in the object plane which requires the sample be surrounded by a support with known transmission properties. For instance, when imaging a biological molecule, it must ideally be either levitating in vacuum or resting on a homogeneous transparent film; both situations are difficult if not impossible to realize. Another problem is the missing signal in the central overexposed region of the diffraction pattern. The intensity ratio between the central spot and the signal at the rim of the detector can reach values of 10^7 ; commonly used 16bit cameras are simply not capable to capture the whole intensity range. Since the higher-order signals provide the desired high-resolution, the central (low-resolution) part is usually sacrificed by being blocked. However, the missing information in the central area is required to initiate the reconstruction with a low-resolution shape of the object. This missing data are usually

obtained by recording a low-resolution image by some other technique, a TEM image for example [4], or by recording a set of images at different exposure times [7, 29].

D. Modified CDI techniques, Fresnel CDI

An intensive search for better techniques has already initiated a number of novel experimental designs, such as Fresnel coherent diffraction imaging [35-38], Fourier transform holography [39-41] and ptychographic coherent diffraction imaging [42-46]. Here we would like to especially mention Fresnel or curved beam coherent diffraction imaging (FCDI) [35-38], since it uses embedded holographic part. FCDI employs a slightly divergent ($1-2^\circ$) beam, which leads to presence of an inline hologram in the center of the diffraction pattern. The available holographic information immediately solves such problems as finding mask for the object support for iterative phase retrieval; it provides fast convergence of the iterative reconstruction and uniqueness of the found solution. However, there are several drawbacks of this method. The average intensity in the central, “holographic”, region is about 10^4 times higher than the intensity of the “diffraction” part of the sample, and to record both parts in one image one would need a set of images under different exposures times (including a very long exposure to record the signal at the rim of the detector). But, since the formed diffraction pattern is not simply Fourier transform of the object function (the incident wavefront is not planar but spherical), it is highly sensitive to any lateral shifts. Thus, a longer acquisition time intended to increase the contrast of higher-order diffraction signals in the diffraction pattern, in fact, just blurs those higher peaks out. Another possibility to record properly both, holographic and diffraction pattern parts in the image, is using a 20bit or higher detector. Finally, the curvature of the incident wave leads to decreased resolution.

III. RELATION BETWEEN INLINE HOLOGRAPHY AND CDI

We address inline holographic scheme because it is relatively easily achieved from CDI experimental scheme by modifying the incident wavefront from parallel into divergent wave. The reconstruction of an object distribution $t(x,y)$ from its inline hologram $H(X,Y)$ requires a deconvolution with the impulse response of a free space propagation factor:

$$S^*(u,v) \text{FT}[H(X,Y)] \approx \text{FT}[t(x,y)] \quad (1)$$

where $S(u,v)$ is the Fourier transform of the free space propagation factor (see Appendix A). On the right side of Eq.(1) is the visibility $V(X,Y)= \text{FT}(t(x,y))$ - the distribution of the scattered wave in the far-field introduced earlier.

In CDI, the measured intensity in the far-field is given by:

$$I(X,Y) = | V(X,Y) |^2 = | \text{FT}(t(x,y)) |^2 \quad (2)$$

Eqs.(1) and (2) demonstrate that the modulus of the Fourier transform of the hologram $| \text{FT}(H(X,Y)) |$ (which we will also call Fourier spectrum of hologram) delivers the amplitude of the scattered object wave in the far-field $| \text{FT}(t(x,y)) |$. In the following we investigate practical consequences of this concept.

Next, we performed set of optical experiments verifying the notion that amplitude of the Fourier spectrum of hologram is indeed the amplitude of the diffraction pattern. The experimental optical scheme which allows an easy alteration between diffraction pattern and hologram acquisition modes is shown in Fig.1. As a test sample we used two tungsten wires of 15 μm diameter twisted around each other, see Fig.2a. The shape of the sample was chosen to mimic DNA double helix structure and thus, to obtain optical

diffraction pattern resembling the famous X-ray fiber diffraction pattern of DNA obtained by Rosalind Franklin. Hologram and diffraction pattern of the sample were recorded and are shown in Fig. 2(b) and (c). Digital Fourier transform of the hologram was calculated and is shown in Fig. 2(d). Fourier spectrum of hologram is missing the higher orders in the spectrum because of the presence noise (see Appendix B). The resolution obtained in hologram can be estimated directly by inspection the highest frequency in the Fourier spectrum of hologram and it corresponds to 6 μm (shown in blue circle). It is obvious that the Fourier spectrum of hologram resembles the measured diffraction pattern shown in Fig. 2(c). Here the diffraction pattern provides the same resolution as the hologram - 6 μm , but it is recorded fulfilling the oversampling condition. These observations lead us to a conclusion that if the oversampling condition is not required for phase retrieval (as it is in the case when the phase is readily accessible from hologram), then the diffraction pattern capturing even *higher* orders of diffraction could be recorded, ultimately resulting in resolution even higher than that obtained by conventional CDI.

We just have shown that (i) a slightly altered experimental CDI scheme can be used to record an inline hologram, and (ii) the amplitude of the Fourier transform of the inline hologram is the same as the amplitude of the diffraction pattern. But there is more to it: the Fourier transform of the hologram is a complex-valued distribution and therefore, its phase part according to Eq.(1) can be used for solving the object structure by iterative reconstruction of diffraction pattern.

IV. HCDI

To set the stage for our HCDI method, we like to start by quoting Gerchberg and Saxton 1972 [13] who made the following comment on using random phase as initial guess in the iterative phase retrieval: “This is not necessary in every case and indeed there is every reason to suppose that an educated guess at the correct phase distribution would lessen the computation time required for the process to achieve an acceptable squared error.”

That was also confirmed by Bates [47] in 1979: “It is seen that availability of even inaccurate phase data can greatly simplify the computational procedure...”

Accurate phase information is exactly what is provided by holography. Thus, in HCDI two images are recorded: a diffraction pattern and an inline hologram of the same object.

The prerequisite of having these two images must not be confused with other methods where also two images are required, as for instance in GS algorithm, where diffraction pattern and low-resolution image of the object are used. Since low-resolution image of object is always a real-valued image, the phase estimate obtained from its Fourier transform will always stagnate the reconstruction process at some real-valued object.

Hence, especially for objects with complex-valued transmission function, a low-resolution image of object cannot be used for guessing the phase distribution in the detector plane. A hologram, in turn, directly contains information on both phase distributions, in the detector plane and in the object plane [48], and therefore, it provides quite an accurate phase estimate for iterative phase retrieval.

A. The central spot

As the Fourier transform of the hologram is the amplitude of the visibility, this feature immediately solves the problem of the usually missing information in the central spot of

the diffraction pattern. It can now directly be obtained from the Fourier spectrum of hologram $| \text{FT}(H(X,Y)) |$.

B. The oversampling condition

Here we would like to recall that Sayre [10] and Bates et al. [24-25] arrived at the “oversampling” condition following the fact that Fourier transform of the measured intensity distribution is the autocorrelation of the object distribution; since the autocorrelation function is always at least twice the size of the object itself, to reconstruct the autocorrelation unambiguously, the intensity of the diffraction pattern must be oversampled by factor 2. In our method the phase of $\text{FT}(H(X,Y)) S^*(u,v)$ provides an accurate estimate of the phase distribution for the iterative reconstruction. Therefore, the oversampling condition becomes obsolete. This can be illustrated by counting the number of unknowns and available equations. The number of unknowns for the real and imaginary parts of the object wave amounts to $2N^2$. The number of equations provided by a holographic measurement is N^2 and that provided by detecting a diffraction pattern is also given by N^2 . Therefore, a hologram and a diffraction pattern together provide matching numbers of equations and unknowns, and thus ensure unique solution. The elimination of the oversampling condition leads to a certain freedom in choice of experimental parameters, which now can be optimized for better resolution, not the oversampling criterion. Next, we show how this available phase information can be fed into the reconstruction routine.

V. HCDI. SIMULATED EXAMPLES

As a test sample, some text was selected, which would allow us visual judging the resolution in the reconstructed images, see Fig. 3(a). The chosen text is a part of Mark Twain's novel "A Fable". Hologram and diffraction pattern were simulated at the parameters that are selected to be realistic and that are later applied in an experimental study. Hologram: wavelength = 532 nm, sample size $1.6 \times 1.6 \text{ mm}^2$, source-sample distance = 5.33 mm, source-screen distance = 1m, screen size = 30 cm. Diffraction pattern: Sample size = $1.6 \times 1.6 \text{ mm}^2$, sample-screen distance = 905 mm and the screen size = 30 cm. All the images were sampled with 1000×1000 pixels².

As it can be seen from the sample structure, shown in Fig.3(a), there is no way of reconstructing diffraction pattern alone, as the oversampling condition is not fulfilled.

Below we suggests two ways (there could be more) of embedding hologram and diffraction pattern into reconstruction routine.

A. Algorithm of Type I. Using phase $S(u,v)FT(H)$ for the first iteration

An obvious way to implement the available phase distribution from hologram is to set it at the beginning of the Fineup's type iterative routine instead of conventionally used random phase distribution. Thus, for the first iteration, the complex-valued visibility is composed as follows: the amplitude is given by the square root of the measured intensity; the phase is given according to Eq.(1) by the phase of $FT(H)S^*(u,v)$, where $S^*(u,v)$ is explained in Appendix A. It amounts to: $\exp((i\pi\lambda D^2)(n^2+m^2)/dS^2)$, where D is the distance between the origin of the spherical wave and the screen, d is the distance

between the source and the object, S is the screen size, and (m,n) denote the pixel positions.

To study the effect of replacing the central part of the diffraction pattern with that of Fourier spectrum of hologram, the central spot of diameter of 22 pixel in the squared root of the diffraction pattern was replaced by the isomorphic central region of the Fourier spectrum of hologram for the first 100 iterations (it was checked that when it is replaced for just one, 1st iteration, or for all the iterations, the result is about the same). For the remaining iterations the central spot was set free from any constraints. The constraints applied in the object domain were selected as following: non-negative absorption constraint was applied to the amplitude distribution [49] and the phase distribution was set free from any constraints. This set of constraints allows recovery of objects with complex-valued transmission function.

The results of the reconstruction after 300 iterations are shown in Fig. 3(b). Without any supporting mask (Fig. 3(b), left) the object text is almost perfectly recovered, though some artefacts remained. With a loose support masks of about 8 pixels from the object contour (Fig. 3(b), right) the recovered object is almost artifact-free. The error function was calculated as:

$$\text{Error} = \frac{\sum ||U_0| - |U_i||}{\sum |U_0|}, \quad (3)$$

where $|U_0|$ is the square root of the measured intensity and $|U_i|$ is the updated amplitude of the complex wave at the detector plane after each iteration. The error function decreases rapidly with the number of iteration followed by an asymptotic approach towards zero, as

displayed in Fig. 3(e), and after 300 iterations it reaches 0.002 and 0.006, with and without masking support, correspondingly.

B. Algorithm of Type II. Using hologram as constraint

Here, the hologram itself is used as a constraint. The complex-valued field in the detector plane in case of inline hologram is given by:

$$U(X, Y) = t(x, y) \otimes s(x, y) \quad (4)$$

where $s(x, y)$ is the free space propagation factor (see Appendix A). Applying the convolution theorem we obtain:

$$\text{FT}[U(X, Y)] = V(u, v) S(u, v) \quad (5)$$

And taking into account that $H(X, Y) = |U(X, Y)|^2$ we re-write:

$$\text{FT}\left[\sqrt{H(X, Y)} e^{i\Psi_H}\right] = |V(u, v)| e^{i(\Psi_V + \Psi_S)} \quad (6)$$

Here Ψ_H , Ψ_V and Ψ_S are the phase distribution in the hologram plane, and of the visibility and $S(u, v)$, correspondingly. Two of these phase distributions, Ψ_H and Ψ_V are not known and can be recovered by running an iterative loop the hologram and diffraction pattern planes. The constraints in the two planes are the measured amplitudes of the complex fields and thus, the classical GS algorithm can be addressed here. Fig. 3(d), left, shows the result of the iterative reconstruction. The reconstruction loop begins from the hologram plane with the initial phase distribution set to 0 (although it was checked that the reconstruction starting from diffraction plane and/or with initial random phase distribution deliver almost identical results). After 200 iterations the object is recognizable but surrounded by artefacts and the error function stagnates, see Fig. 3(e).

Unfortunately, a hologram often does not contain high-resolution information, and therefore using hologram as a constraint might blur and lead to artefacts in the reconstruction. To improve the situation, the recovered complex-valued visibility (the result of the first iterative run multiplied with $S^*(u,v)$) can be refined by another iterative run between diffraction pattern and the object planes. The results of the second iterative run of 600 iterations are shown in Fig. 3(d), right. Here, the constraint in the object plane was only the non-negative absorption, no supporting masks were used. The reconstructed object is arte-fact free, and the error function drops to 0.0002 after 800 iterations in total. We have given prescription for at least two possible ways to recover a non-oversampled diffraction pattern when an additional inline hologram of the sample is available.

VI. HCDI. EXPERIMENTAL EXAMPLES

A. Optical experiments

An optical setup employing laser light of 532 nm wavelength has been used. It allows recording a hologram and a diffraction pattern of the same object without significant modification, as shown in Fig. 1: only the illuminating wavefront is converted from a parallel into a spherical one. As for the objects, two objects were selected: (i) A knotted hair due to its simple geometry and easy-to-interpret diffraction pattern, and (ii) A wing of a fly, which results in a structureless diffraction pattern.

Figure 4 shows the hologram (Fig. 4(b)) and the diffraction pattern (Fig. 4(c)) of the knotted hair. The squared amplitude of the Fourier transform of the hologram, displayed in Fig. 4(e), exhibits a distribution which compares well to the measured diffraction pattern shown in Fig. 4(d). The low-order modulations in $|\text{FT}(H(X,Y))|$ and in the

diffraction pattern are found at the same positions. The higher order diffraction peaks are absent in $|\text{FT}(H(X,Y))|$ because of experimental noise in the reference wave. A hologram can be reconstructed on its own, and the results of such reconstructions are displayed in Fig. 4(e) and (f). The details in these hologram reconstructions are blurred and the presence of the out-of-focus twin images is apparent.

The recorded diffraction pattern was reconstructed using the phase information available from hologram, as described in above in algorithm of Type I. For the first loop of the iterative retrieval procedure the complex-valued distribution in the detector plane is composed from the measure amplitude and phase of $\text{FT}(H)S^*(u,v)$. This phase distribution is used only for the first iteration. The missing central region of 18 pixels in diameter is filled with the amplitude distribution of $\text{FT}(H)$ for the first 100 iterations. A non-negative absorption constraint [49] and a loose support mask of about 20 pixels from the object contour are applied in the object plane. A recognizable object distribution has already been achieved just after the first iteration. The amplitude and phase distributions retrieved after 300 iterations are shown in Fig. 4(g) and (h). Fine details of about 1 pixel in size (corresponding to $1.6\mu\text{m}$) can be resolved in the reconstruction displayed in Fig. 4(g).

Another application of the HCDI method is shown in Fig. 5. This time, the object, a wing of a small fly, was selected for the sake of obtaining a structure-less diffraction pattern without distinct peaks. Again, the measured diffraction pattern and the squared amplitude of the Fourier transform of the hologram are visually identical. The amplitude and phase distributions retrieved after 300 iterations by the same HCDI iterative procedure as described above are shown in Fig. 5(e) and (f).

B. Low-energy electron experiment

We also tested HCDI method on images recorded with low-energy electrons. The sample was multi-walled carbon nanotubes stretched over holes milled in a carbon film, prepared in a manner described elsewhere [50]. The experimental setup available in our laboratory is sketched in Fig. 6(a); the transition from a spherical to a plane wavefront was realized by adjusting the voltage of the focusing micro-lens [50-51]. Hologram was recorded with electrons of 51 eV energy and is shown in Fig. 6(b); the distance between the electron source and the sample was 640 nm. The diffraction pattern is composed from 4 images recorded with electrons of 145 eV energy, at different exposure times: 4, 8, 16 and 32 seconds, shown in Fig.6(c). The central part is missing and adapted from $FT(H)$. Both, the hologram and the diffraction pattern are sampled with 1200×1200 pixels². The images were reconstructed by an iterative procedure with 300 iterations as described above in optical experiments section, where the central spot of 60 pixels in diameter was replaced for the first 100 iterations. The resulting reconstruction, shown in Fig. 6(d) is in a good agreement with TEM image displayed in Fig. 6(e).

VII. DISCUSSION

We have demonstrated that an inline hologram can be recorded in a modified CDI experimental scheme. The amplitude of the Fourier transform of the inline hologram is the same as the amplitude of the diffraction pattern and its phase provides an accurate guess for phase retrieval routine. With the good phase guess, the condition of oversampling of diffraction patterns becomes obsolete. Thus, the experimental parameters must not anymore be selected to fulfil the oversampling condition, but instead

they can be selected to achieve highest possible resolution. We suggested two recipes of implementing phase information into phase retrieval routine. In Type I algorithm, $FT(H)$ is only used for the first iteration. In Type II algorithm, the hologram itself serves as a constraint. Although we have demonstrated the HCDI method using light optics and low-energy electrons, it can obviously also be applied to other coherent radiation such as X-rays or high-energy electrons with an expected resolution scaling with the wavelength. The holographic acquisition scheme can be realized in X-ray diffraction experiments either by shifting the Fresnel zone plate or the object, thus placing the object into a divergent beam. For future experiments, as the information stored in a holographic image is actually three-dimensional, the method might be extended to reconstruct the three-dimensional structure of objects from their diffraction patterns.

ACKNOWLEDGEMENTS

The authors would like to acknowledge the assistance of Conrad Escher for the sample preparation. We would also like to thank Mirna Saliba for careful reading of the manuscript. The “Forschungskredit of the University of Zurich” as well as the Swiss National Science Foundation are gratefully acknowledged for their financial support.

APPENDIX A: HOLOGRAM FORMATION AND RECONSTRUCTION

The transmission function in the object plane can be written as:

$$t(x,y) = 1 + o(x,y) = \exp(-a(x,y)) \exp(-i\phi(x,y)) \quad (\text{A1})$$

where $a(x,y)$ and $\phi(x,y)$ describe absorbing and phase shifting properties in some plane in the object domain. An incident spherical wave passing the object is described by $(1/z_0)\exp(i\pi/\lambda z_0(x^2+y^2))$, where z_0 is the distance between the origin of the wave and the object. The scattered wave in the detector plane is represented as:

$$U(X,Y) = -\frac{i}{\lambda z_0 z_s} \iint t(x,y) \exp\left(\frac{i\pi}{\lambda z_0}(x^2+y^2)\right) \exp\left(\frac{i\pi}{\lambda z_s}\left((x-X)^2+(y-Y)^2\right)\right) dx dy \quad (\text{A2})$$

Here, z_s is the distance between object and detector, and (X,Y) denote coordinates in the detector plane. The intensity in the detector plane, and thus the hologram distribution, is given by:

$$H(X,Y) = |U(X,Y)|^2 = \frac{1}{(\lambda z_0 z_s)^2} \left| \iint t(x,y) \exp\left(\frac{i\pi}{\lambda z_0}\left(\left(x-X\frac{z_0}{z_s}\right)^2 + \left(y-Y\frac{z_0}{z_s}\right)^2\right)\right) dx dy \right|^2. \quad (\text{A3})$$

The expression under the integral can be represented as a convolution and leads to the following expression after hologram normalization (division by the intensity of the wave at the detector in the absence of the object)[52]:

$$H(X,Y) = |t(X,Y) \otimes s(X,Y)|^2 \quad (\text{A4})$$

in which we introduced the Fresnel function:

$$s(x, y) = -\frac{i}{\lambda z_0} \exp\left(\frac{i\pi}{\lambda z_0}(x^2 + y^2)\right) \quad (\text{A5})$$

Its Fourier transform $S(u, v)$ is given by:

$$S(u, v) = -\frac{i}{\lambda z_0} \iint \exp\left(\frac{i\pi}{\lambda z_0}(x^2 + y^2)\right) \exp(-2\pi i(xu + yv)) dx dy = \exp(-i\pi\lambda z_0(u^2 + v^2)) \quad (\text{A6})$$

The hologram distribution in Eq.(A4) can be rewritten as:

$$H(X, Y) = \left| (1 + o(X, Y)) \otimes s(X, Y) \right|^2 \quad (\text{A7})$$

Taking into account that

$$1 \otimes s(X, Y) = -\frac{i}{\lambda z_0} \iint \exp\left(\frac{i\pi}{\lambda z_0}((x-X)^2 + (y-Y)^2)\right) dx dy = 1 \quad (\text{A8})$$

we expand the hologram distribution as:

$$H(X, Y) = 1 + o(X, Y) \otimes s(X, Y) + o^*(X, Y) \otimes s^*(X, Y) + |o(X, Y) \otimes s(X, Y)|^2 \quad (\text{A9})$$

Since we know from inline holography reconstruction that the first two terms represent the dominant information on the object, for further discussion we are neglecting the conjugate term and the small perturbation term:

$$H(X, Y) \approx 1 + o(X, Y) \otimes s(X, Y) \quad (\text{A10})$$

Reconstructing the hologram includes three steps. 1. It begins with calculating its Fourier transform:

$$\text{FT}[H(X, Y)] \approx \delta(u, v) + O(u, v)S(u, v) \quad (\text{A11})$$

2. It is then followed by multiplying with $S^*(u, v)$ and using $|S(u, v)|^2 = 1$:

$$S^*(u, v)\text{FT}[H(X, Y)] \approx S^*(u, v)\delta(u, v) + O(u, v) \quad (\text{A12})$$

3. Finally, the result is backward Fourier-transformed:

$$\text{FT}^{-1}\{S^*(u, v)\text{FT}[H(X, Y)]\} = 1 + o(x, y) \quad (\text{A13})$$

where we used:

$$\iint S^*(u, v)\delta(u, v)\exp(2\pi i(xu + yv))dx dy = 1. \quad (\text{A14})$$

Next, we would like to point out that according to Eq.(A13), the following equation

applies:

$$S^*(u, v)\text{FT}[H(X, Y)] = \text{FT}[t(x, y)] \quad (\text{A15})$$

where $\text{FT}[t(x, y)]$ is also the visibility $V(X, Y) = \text{FT}(t(x, y))$ – the distribution of the scattered wave in the far-field.

APPENDIX B: RESOLUTION IN INLINE HOLOGRAPHY

Resolution in inline holography can be studied on example of hologram of a point scatterer. An ideal noise-free inline hologram of a point-scatterer is practically, a Fresnel zone plate (FZP). Such a hologram, when recorded on an infinite large screen, gives image of δ -function in the reconstruction. However, in reality, the limited sizes of both the screen and the detector pixel lead to the limited resolution. The finest resolved fringes in the formed hologram define the resolution.

Fourier spectrum of an inline hologram of an object to a good approximation is diffraction pattern of the object, placed at a distance z_1 from the screen of size $S_0 = \lambda z_s N / S_H$. Here, z_s is the distance between the source of the divergent wave and the screen, S_H is the screen size and N – number of pixels.

For large distances z_1 , i.e. small magnification $M = z_s / z_1$, the formed hologram is a FZP with very high NA, and thus the challenge is to resolve the outermost fine fringes whose width is comparable to the detector pixel size. According to the Shannon sampling theorem, it requires at least 2 samplings per period to correctly represent a periodic signal. It means that the finest resolved fringe must have period of 2 pixels, independent on the size of pixel. For any periodic signal of period T_p (in pixels), in the Fourier spectrum the peaks at $\nu_p = \pm N / T_p$ are observed. Thus, for $T_p = 2$ (in pixels), the corresponding peaks in the Fourier spectrum are found at $\nu_p = \pm N / 2$ (in pixels). The positions of these peaks define the resolution limited due to the sampling R_s : $R_s = 2\lambda z_1 / S_0$, or when substituting S_0 defined above:

$$R_s = 2 \frac{\lambda z_1 S_H}{z_s N} \quad (\text{B1})$$

The resolution R_S is linearly increasing with z_1 .

However, the finest fringes such as those which have period of 2 pixels only, are very difficult to be distinguished from the experimental noise. In practice, the Fourier spectrum of hologram always shows limited resolution $R_{\text{exp}} < R_S$.

As the distance z_1 gets shorter, the finest fringes get larger and take up more than 2 pixels per period. The maxima in the hologram of a points scatterer are distributed as:

$$\frac{\pi z_1}{\lambda z_s^2} x_s^2 = 2\pi q, \dots \quad q = 0, 1, 2, \dots \quad (\text{B2})$$

Where x_s is the coordinate on the screen and it can range in the limits $x_s = 0 \dots S_H$. The distance between two maxima of the finest fringes is given by:

$$T = z_s \sqrt{\frac{2\lambda}{z_1} (\sqrt{Q} - \sqrt{Q-1})} \approx \frac{\lambda z_s^2}{z_1 S_H} \quad (\text{B3})$$

here Q is the number of the finest fringe. This period in pixels $T_p = TN/S_H$ defines the position of the corresponding peak in Fourier domain: $v_p = \pm N/T_p$ (in pixels), and leads to the following resolution in the reconstructed object:

$$R_G = T_p \frac{s_1}{N} = \frac{\lambda z_s}{S_H} \quad (\text{B4})$$

Where $s_1 = z_1 S_H / z_s$ is the size of the reconstructed area. The resolution R_G does not depend on the source-sample distance z_1 but depends on source-screen distance z_s , screen size S_H and the wavelength λ . Thus, this resolution is only limited by the geometry of the setup and hence, named R_G .

To verify the experimentally obtainable resolution in inline holograms, 11 optical holograms of twisted tungsten wires at different z_1 distances but the same source-screen

distance $z_s = 10\text{cm}$ and the screen size $S_H = 25\text{mm}$ were recorded. Three of these holograms are shown in Fig.7. The highest detected frequency in the Fourier spectrum of hologram (shown as blue circles in Fig.7(a)-(c)) defines the experimental resolution R_{exp} which is calculated as

$$R_{\text{exp}} = 2 \frac{\lambda z_1 S_H}{S_0^*}, \quad (\text{B5})$$

where S_0^* is the “effective screen” corresponding to the area where the signal in the Fourier spectrum is observed (the area within blue circles). The estimated resolution R_{exp} is plotted against z_1 in graph Fig. 7(d). The resolution limited by the sampling R_S is shown as red circles in the Fourier spectra and as red line in the graph in Fig. 7(d). The resolution provided by the geometry of the setup is shown as green line in Fig. 7(d).

The following can be concluded by studying the results presented in Fig.7:

- (i) The resolution of an inline hologram can be directly evaluated from its Fourier spectrum
- (ii) At large source-sample distances z_1 the resolution is limited by the sampling of hologram
- (iii) At small source-sample distances z_1 the resolution is limited by the geometry of the setup.

References

- [1] D. Gabor, *A new microscopic principle*, Nature **161**, 777 (1948).
- [2] J. W. Miao *et al.*, *Extending the methodology of X-ray crystallography to allow imaging of micrometre-sized non-crystalline specimens*, Nature **400**, 342 (1999).
- [3] D. Gabor, *Microscopy by reconstructed wave-fronts*, Proc. Phys. Soc. London. Series A **197**, 454 (1949).
- [4] J. M. Zuo *et al.*, *Atomic resolution imaging of a carbon nanotube from diffraction intensities*, Science **300**, 1419 (2003).
- [5] J. R. Fienup, *Phase retrieval algorithms - a comparison*, Appl. Optics **21**, 2758 (1982).
- [6] J. W. Miao *et al.*, *Imaging whole Escherichia coli bacteria by using single-particle x-ray diffraction*, Proc. Natl. Acad. Sci. U. S. A. **100**, 110 (2003).
- [7] D. Shapiro *et al.*, *Biological imaging by soft x-ray diffraction microscopy*, Proc. Natl. Acad. Sci. U. S. A. **102**, 15343 (2005).
- [8] C. Y. Song *et al.*, *Quantitative imaging of single, unstained viruses with coherent X-rays*, Phys. Rev. Lett. **101**, 158101 (2008).
- [9] M. M. Seibert *et al.*, *Single mimivirus particles intercepted and imaged with an X-ray laser*, Nature **470**, 78 (2011).
- [10] D. Sayre, *Some implications of a theorem due to Shannon*, Acta Crystallogr. **5**, 843 (1952).
- [11] C. E. Shannon, *Communication in the Presence of Noise*, Proc. IEEE **86**, 447 (1949).
- [12] D. Sayre, *X-ray crystallography: The past and present of the phase problem*, Struct. Chem. **13**, 81 (2002).
- [13] R. W. Gerchberg, and W. O. Saxton, *A practical algorithm for determination of phase from image and diffraction plane pictures*, Optik **35**, 237 (1972).
- [14] R. H. T. Bates, *On phase problems I*, Optik **51**, 161 (1978).
- [15] J. R. Fienup, *Reconstruction of an object from modulus of its Fourier-transform*, Opt. Lett. **3**, 27 (1978).
- [16] S. Marchesini *et al.*, *X-ray image reconstruction from a diffraction pattern alone*, Phys. Rev. B **68** (2003).
- [17] T. Latychevskaia, J. N. Longchamp, and H. W. Fink, *Novel Fourier-domain constraint for fast phase retrieval in coherent diffraction imaging*, Opt. Express **19**, 19330 (2011).
- [18] N. Wiener, *Generalized harmonic analysis*, Acta Mathematica **55** (1930).
- [19] A. Chintchin, *Korrelationstheorie der stationären stochastischen Prozesse*, Mathematische Annalen **109** (1934).
- [20] E. M. Hofstetter, *Construction of time-limited functions with specified auto-correlation functions*, IEEE Transactions on Information Theory **10**, 119 (1964).
- [21] A. M. J. Huiser, A. J. J. Drenth, and H. A. Ferwerda, *On phase retrieval in electron-microscopy from image and diffraction pattern*, Optik **45**, 303 (1976).
- [22] A. M. J. Huiser, and H. A. Ferwerda, *On the problem of phase retrieval in electron microscopy from image and diffraction pattern. 2. Uniqueness and stability.*, Optik **46**, 407 (1976).

- [23] Y. M. Bruck, and L. G. Sodin, *On the ambiguity of the image reconstruction problem*, Opt. Commun. **30**, 304 (1979).
- [24] R. H. T. Bates, *Fourier phase problems are uniquely solvable in more than one dimension I. underlying theory*, Optik **61**, 247 (1982).
- [25] R. H. T. Bates, *Uniqueness of solutions to two-dimensional Fourier phase problems for localized and positive images*, Computer Vision Graphics and Image Processing **25**, 205 (1984).
- [26] R. P. Millane, *Multidimensional phase problems*, J. Opt. Soc. Am. A-Opt. Image Sci. Vis. **13**, 725 (1996).
- [27] J. R. Fienup, and C. C. Wackerman, *Phase-retrieval stagnation problems and solutions*, J. Opt. Soc. Am. A - Opt. Image Sci. Vis. **3**, 1897 (1986).
- [28] W. J. Huang *et al.*, *Towards sub-Å atomic resolution electron diffraction imaging of metallic nanoclusters: A simulation study of experimental parameters and reconstruction algorithms*, Ultramicroscopy **107**, 1159 (2007).
- [29] P. Thibault, and I. C. Rankenburg, *Optical diffraction microscopy in a teaching laboratory*, Am. J. Phys. **75**, 827 (2007).
- [30] K. S. Raines *et al.*, *Three-dimensional structure determination from a single view*, Nature **463**, 214 (2010).
- [31] R. Barakat, and G. Newsam, *Necessary conditions for a unique solution to two-dimensional phase recovery*, J. Math. Phys. **25**, 3190 (1984).
- [32] R. H. T. Bates, and D. G. H. Tan, *Fourier phase retrieval when the image is complex*, Inverse Optics II, Proc. SPIE **558**, 54 (1985).
- [33] J. R. Fienup, *Reconstruction of a complex-valued object from the modulus of its Fourier-transform using a support constraint*, J. Opt. Soc. Am. A - Opt. Image Sci. Vis. **4**, 118 (1987).
- [34] U. Weierstall *et al.*, *Image reconstruction from electron and X-ray diffraction patterns using iterative algorithms: experiment and simulation*, Ultramicroscopy **90**, 171 (2002).
- [35] G. J. Williams *et al.*, *Fresnel coherent diffractive imaging*, Phys. Rev. Lett. **97**, 025506 (2006).
- [36] G. J. Williams *et al.*, *Curved beam coherent diffractive imaging*, Thin Solid Films **515**, 5553 (2007).
- [37] L. W. Whitehead *et al.*, *Fresnel diffractive imaging: Experimental study of coherence and curvature*, Phys. Rev. B **77**, 104112 (2008).
- [38] G. J. Williams *et al.*, *Fresnel coherent diffractive imaging: treatment and analysis of data*, New J. Phys. **12**, 035020 (2010).
- [39] I. McNulty *et al.*, *High-resolution imaging by Fourier-resolution imaging by Fourier-transform X-ray holography*, Science **256**, 1009 (1992).
- [40] S. Eisebitt *et al.*, *Lensless imaging of magnetic nanostructures by X-ray spectro-holography*, Nature **432**, 885 (2004).
- [41] S. Marchesini *et al.*, *Massively parallel X-ray holography*, Nature Photon. **2**, 560 (2008).
- [42] P. Thibault *et al.*, *High-resolution scanning x-ray diffraction microscopy*, Science **321**, 379 (2008).

- [43] D. J. Vine *et al.*, *Ptychographic Fresnel coherent diffractive imaging*, Phys. Rev. A **80** (2009).
- [44] P. Thibault *et al.*, *Probe retrieval in ptychographic coherent diffractive imaging*, Ultramicroscopy **109**, 338 (2009).
- [45] A. M. Maiden, and J. M. Rodenburg, *An improved ptychographical phase retrieval algorithm for diffractive imaging*, Ultramicroscopy **109**, 1256 (2009).
- [46] M. Dierolf *et al.*, *Ptychographic X-ray computed tomography at the nanoscale*, Nature **467**, 436 (2010).
- [47] R. H. T. Bates, *On phase problems II*, Optik **51**, 223 (1978).
- [48] T. Latychevskaia, and H.-W. Fink, *Simultaneous reconstruction of phase and amplitude contrast from a single holographic record*, Opt. Express **17**, 10697 (2009).
- [49] T. Latychevskaia, and H.-W. Fink, *Solution to the twin image problem in holography*, Phys. Rev. Lett. **98**, 233901 (2007).
- [50] E. Steinwand, J.-N. Longchamp, and H.-W. Fink, *Coherent low-energy electron diffraction on individual nanometer sized objects*, Ultramicroscopy **111**, 282 (2011).
- [51] E. Steinwand, J. N. Longchamp, and H. W. Fink, *Fabrication and characterization of low aberration micrometer-sized electron lenses*, Ultramicroscopy **110**, 1148 (2010).
- [52] J. C. H. Spence, X. Zhang, and W. Qian, in *Electron Holography*, edited by L. F. A. A. Tonomura, G. Pozzi, D. C. Joy and Y. A. Ono (Elsevier Science, 1995).

Figures

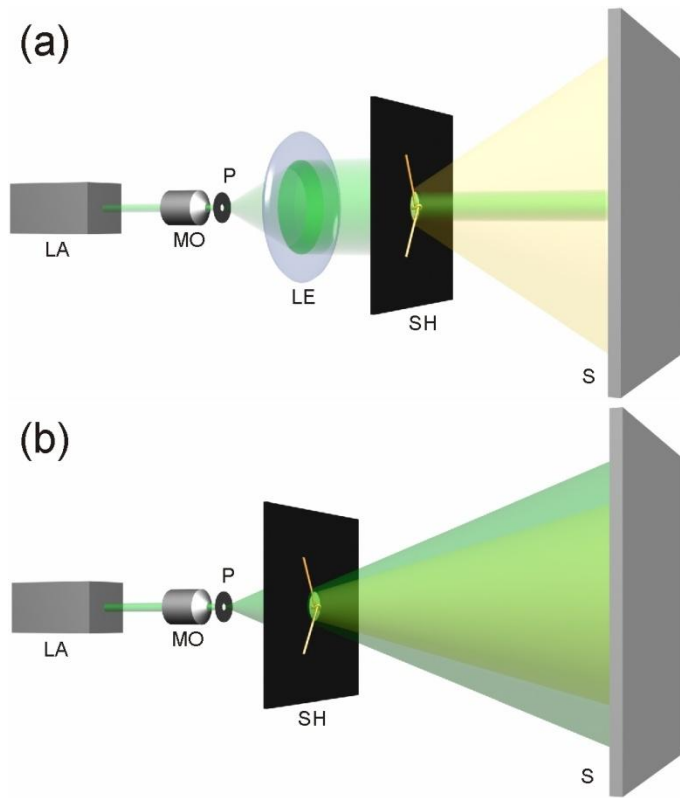


FIG. 1. Optical schemes. (a) Scheme for recording diffraction patterns. Laser light from the laser source (LA) passes the spatial filtering system (microscope objective (MO) with a $NA=0.85$ and pinhole (P) of diameter = $10\ \mu\text{m}$). The object is fixed at the sample holder (SH). For the recording of diffraction patterns, the wavefront is broadened by a lens (LE). (b) Scheme for recording holograms. The lens LE is removed and the sample is shifted closer to the pinhole P. Both, diffraction patterns and holograms are recorded by 10bit CCD camera with 1000×1000 pixels.

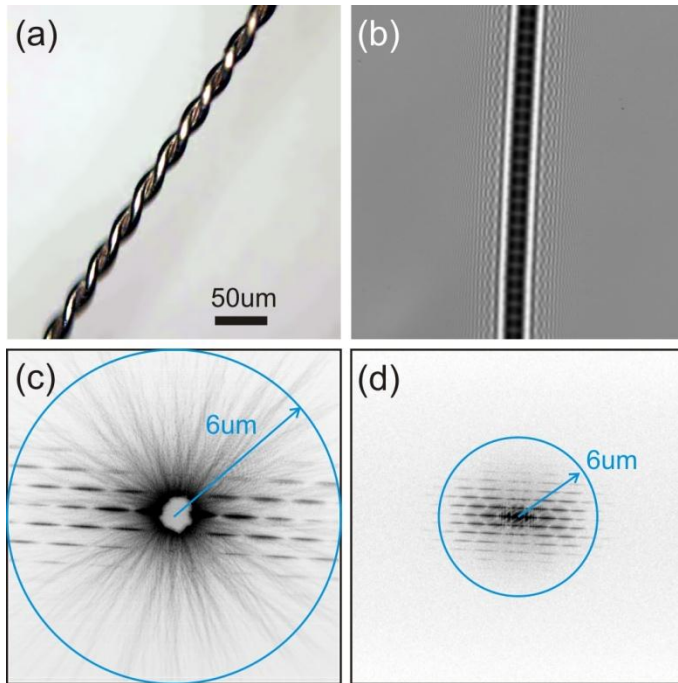
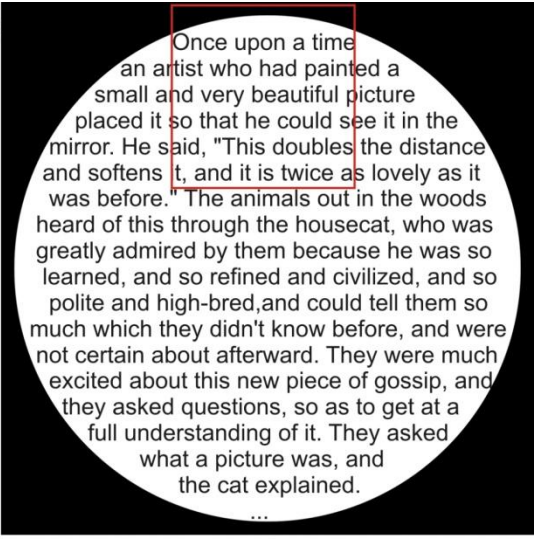
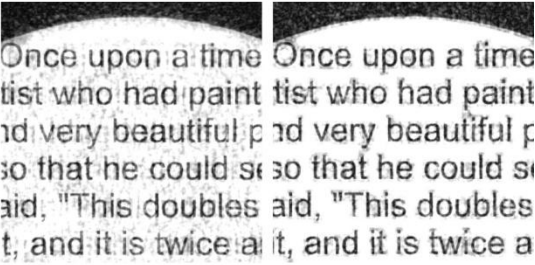
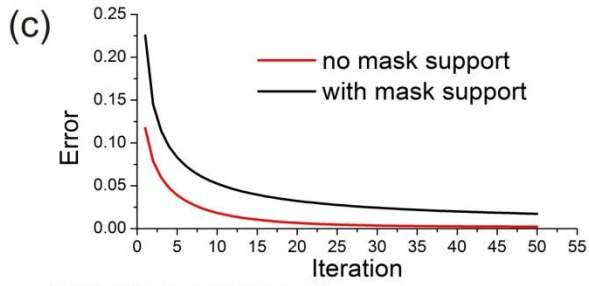
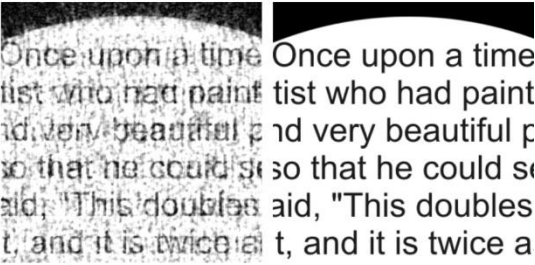


FIG. 2. Experimental verification of the relation between hologram and diffraction pattern. (a) Reflected-light microscopy image of twisted tungsten wires. (b) Hologram recorded using the scheme shown in Fig.1(b) at the pinhole-screen distance 100 mm and the pinhole-sample distance 5.8 mm. (c) Diffraction pattern recorded using the scheme shown in Fig.1(a) at the sample-screen distance 145 mm. For both (b) and (c) the screen size was $25 \times 25 \text{ mm}^2$, and the images were sampled with $1000 \times 1000 \text{ pixels}^2$. (d) Amplitude of Fourier transform of hologram shown in logarithmic and inverted intensity scale.

(a) 

(b) 



(d) 

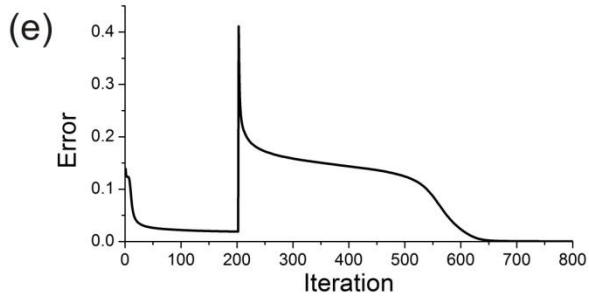


FIG. 3 Simulated study of the HCDI method. (a) The transmission function of the sample in form of the text. The part of the sample marked by the red square is shown in the reconstruction below. (b) Reconstruction obtained by using Type I algorithm shown after 300 iterations. Left: No supporting mask was employed. Right: Supporting mask was employed for all iterations. (c) Error as function of the iteration number shown for the first 50 iterations of (b). (d) Reconstruction obtained by using Type II algorithm. Left: after 200 iterations ran between hologram and diffraction pattern planes. Right: After additional 600 iterations ran between diffraction pattern and object planes. (e) Error as function of the iteration number for reconstruction in (d).

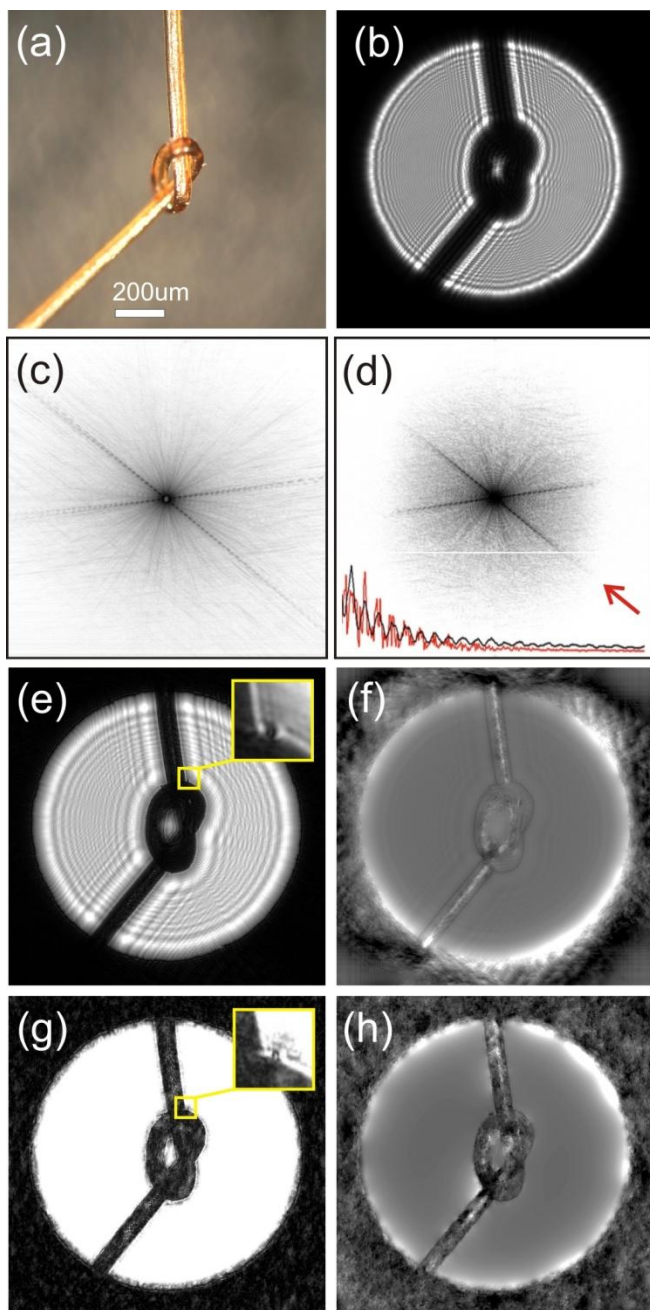


FIG. 4. HCDI reconstructions of a human hair. (a) Reflected-light microscopy image of a hair. (b) Recorded hologram: the pinhole-sample distance amounts to 5.3 mm. (c) Experimental diffraction pattern recorded at 1 m from the sample. (d) Amplitude of the Fourier transform of the hologram. The inset shows the profiles of the square root of the experimental diffraction pattern intensity (black) and the amplitude of $FT(H)$ (red) along

the direction indicated by a red arrow. The resolution provided in a hologram can be estimated by examining the amplitude of $FT(H)$, and it is usually less than the resolution provided in the diffraction pattern. (e) Amplitude distribution reconstructed from the hologram. The superimposed interference pattern arises from the twin image. In the inset, a magnified 40x40 pixels part of the reconstruction is shown. (f) Phase distribution reconstructed from hologram. (g) Amplitude distribution reconstructed with HCDI. The inset shows a magnified 40x40 pixels part of the reconstruction, demonstrating an improved resolution when comparing to the hologram reconstruction. (h) Phase distribution reconstructed with HCDI.

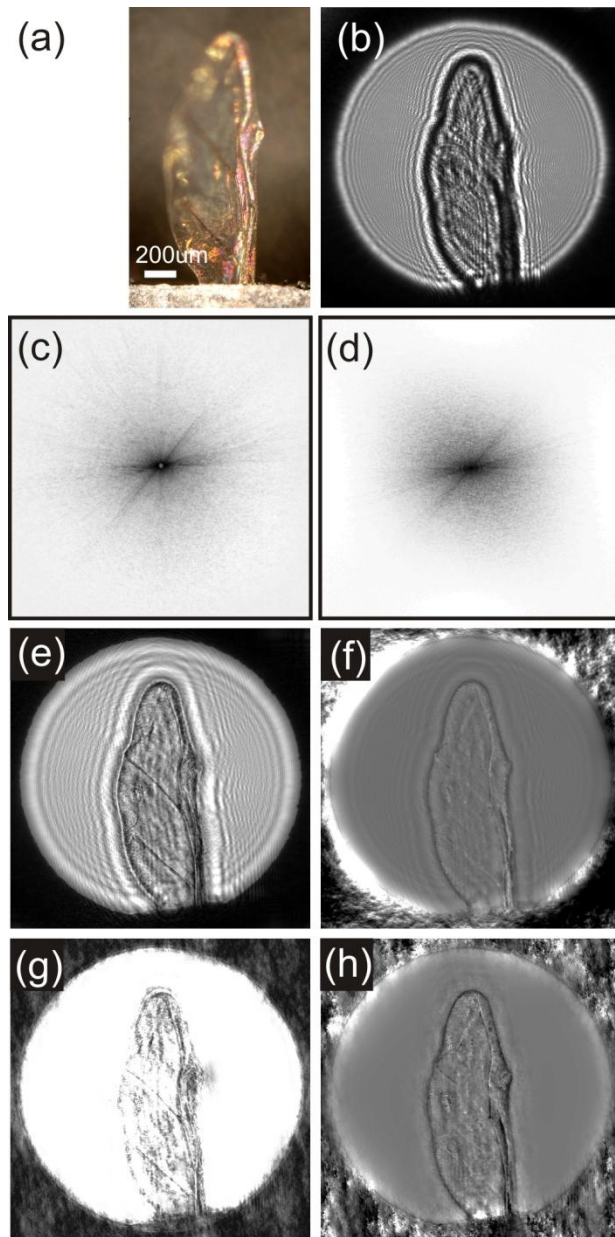


FIG. 5. HCDI reconstructions of a fly wing. (a) Reflected-light microscopy image of a small fly wing. (b) Recorded hologram: the pinhole-sample distance amounts to 5.3 mm. (c) Experimental diffraction pattern recorded at 1 m from the sample. (d) Amplitude of $FT(H)$. (e) Amplitude distribution reconstructed from the hologram. (f) Phase distribution reconstructed from the hologram. (g) Amplitude distribution reconstructed with HCDI. (h) Phase distribution reconstructed with HCDI.

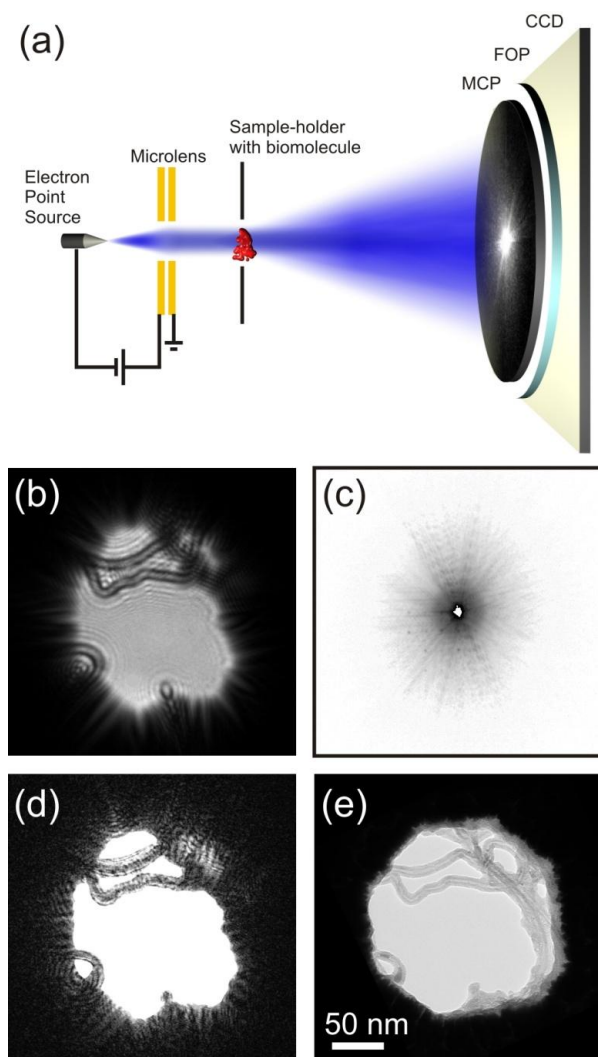


FIG. 6. HCDI reconstructions of a coherent low-energy electron images of individual carbon nanotubes. (a) Schematics of home-built low-energy electron microscope, the distance between the electron source and the detector is 10 cm. The detector components are: micro-channel plate (MCP), fiber optical plate (FOP) and CCD chip. (b) Hologram recorded with electrons of 51 eV energy. In (b) and (d) the central parts of images, size of 600x600 pixels are shown. (c) Diffraction pattern recorded with electrons of 145 eV energy. (d) Amplitude distribution reconstructed by HCDI. (e) TEM image recorded with 200 keV electrons.

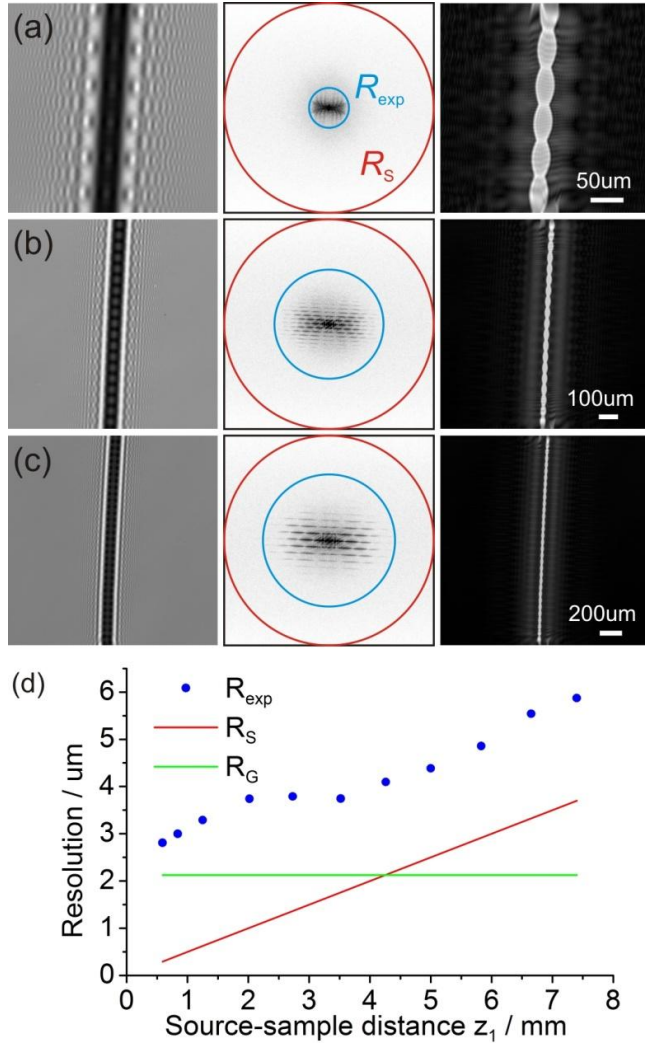


FIG. 7. Sequence of 11 optical holograms of twisted tungsten wires recorded with 532 nm laser light, at source sample distance 10cm, screen size 25 mm, and different source-sample z_1 distances. Three of the holograms shown in the left column are recorded at the following source-sample distances: (a) 1.25 mm, (b) 3.50 mm and (c) 7.40 mm. The images in the center column show the inverted amplitude of the Fourier spectra of the corresponding holograms (in logarithmic intensity scale). Red circles show the resolution limited by the digital sampling R_S . Blue circles show the resolution corresponding to the highest observed frequency in the Fourier spectrum. The images in the right column show

the reconstructed object. (d) Plot of resolution as function of source-sample distance.

Blue dots correspond to the experimental resolution R_{exp} , as for instance, the resolution corresponding to the blue circles in (a)-(c). The red line shows the resolution limit R_S due to the sampling. The green line shows the resolution R_G limited by geometry of the setup.